First Order Perturbative Effect of Earth's Rotation on GW Signal Model

Samyak Tiwari

July 9, 2025

Abstract

Michelson interferometry is a laboratory technique that is used for several experiments - forming interference patterns to determine the wavelength of light, studying wind and temperature patterns in the upper atmosphere, and detecting gravitational waves with LIGO. This report explores the latter application; in particular, a first-order approximation of the effect of Earth's rotation on the gravitational wave (GW) signals received by LIGO. This approximation is of pressing significance to next-generation detectors, whose longer readable signal lengths require consideration of Earth's rotation for proper parameter estimation. This report includes a brief background of the general relativity theory underlying GWs, an account of the current LIGO detector setup and the GW model it uses, and a far more detailed account of the first-order expansion on the existing gravitational wave signal model. Finally, the report concludes with a discussion of Bayesian techniques for parameter estimation on noisy raw data and further possible works.

Table of Contents

1 Introduction

When Albert Michelson invented the interferometer in 1881, he hadn't imagined the scale at which it would be used. Designed initially to probe the wave-like nature of light, his invention laid the groundwork for some of the most precise measurement tools in physics. Over time, the interferometer evolved from a tabletop apparatus to a kilometer-scale scientific instrument. Its journey mirrors the trajectory of modern physics itself, from classical mechanics to the frontier of general relativity.

1.1 The Gravitational Wave (GW)

Gravitational waves are spacetime ripples produced by accelerating masses, with compact binary mergers—black holes or neutron stars—among the only sources powerful enough to be detected by LIGO. When two such masses orbit each other, they lose energy to gravitational radiation, and their orbits shrink while their inspiral frequency rises. This makes the gravitational wave signal "chirp" as its frequency and amplitude rise leading to the point of merger, manifesting as perturbations in spacetime.

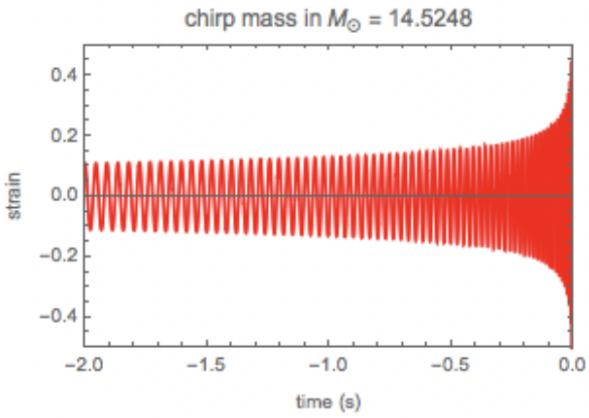

Figure 1: GW Signal Example.[4]

In the linearized theory of general relativity, the spacetime metric $g_{\mu\nu}$ represents the perturbed Minkowski metric $\eta_{\mu\nu}$. That is,

$$g_{\mu\nu} = \eta_{\mu\nu} + h_{\mu\nu}, \quad |h_{\mu\nu}| \ll 1 \tag{1}$$

The perturbation $h_{\mu\nu}$ takes a particularly convenient form for a wave propagating in the z-direction:

$$h_{\mu\nu} = \begin{pmatrix} 0 & 0 & 0 & 0 \\ 0 & h_+ & h_\times & 0 \\ 0 & h_\times & -h_+ & 0 \\ 0 & 0 & 0 & 0 \end{pmatrix}$$

This form reveals two independent polarization modes of the gravitational wave (see Figure 1):

- h_+: the *plus* polarization, which stretches and compresses spacetime along the x- and y-axes.
- $h_\times$: the *cross* polarization, oriented at 45 degrees to the plus mode.

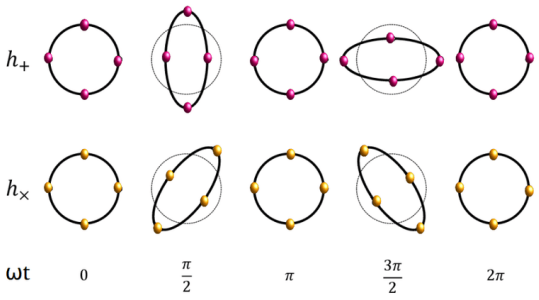

Figure 2: Illustration of gravitational wave polarizations along transverse plane: h_+ and $h_\times$.[1]

Both modes are transverse to the direction of wave propagation (along the z-axis). This is characteristic of gravitational radiation in free space.

2 Current GW Signal Model

2.1 What is an interferometer?

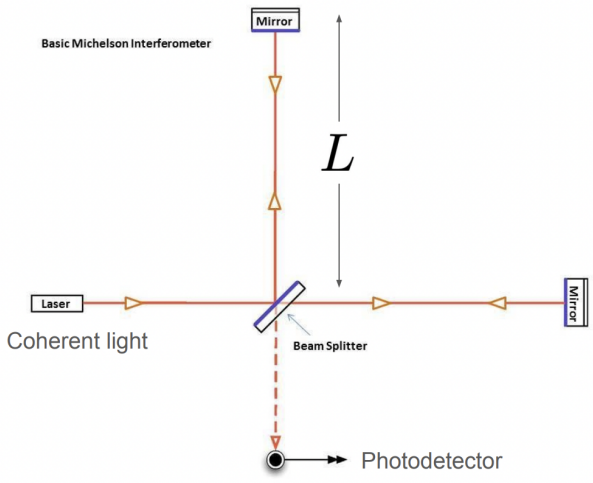

Figure 3: Standard Michelson Interferometer. L is the length of the interferometer's arms. [3]

An interferometer is a scientific instrument that uses the principle of interference to make precise measurements of displacement. In the case of a Michelson Interferometer, such as those used in LIGO, laser light is split into two beams that travel along perpendicular arms. These beams are reflected back by mirrors and recombined at the photodetector. The resulting interference pattern depends on the difference in the path lengths traveled by the two beams.

The path length difference ΔL between the arms is related to the measured phase difference $\Delta\phi$ by:

$$\Delta L = \frac{\lambda\,\Delta\phi}{2\pi} \tag{2}$$

where λ is the wavelength of the light beam used in the experimental setup.

At its most sensitive state, LIGO is able to detect a change in distance between its mirrors 1/10,000th the width of a proton (10^{-19} m) across its 4km arms [3]! Streams of strain data $h = \Delta L/L$ are noise-reduced (primarily via high-pass filtering) and compared with a template bank of various simulated GW signals to detect merger events.

2.2 How are multiple interferometers used?

LIGO-Livingston, LIGO-Hanford, and Virgo are used together for coincidence detection (that is, to ensure that a real astrophysical event is being observed) and to determine the sky location of an observed event. Each detector's axis orientation determines its sensitivity to the "+" (plus) and "×" (cross) polarization modes of the wave, which are described by the detector-specific response functions F_+ and $F_\times$, respectively. F_+ and $F_\times$ depend on Φ, the sky angle δ, and the polarization angle ψ.

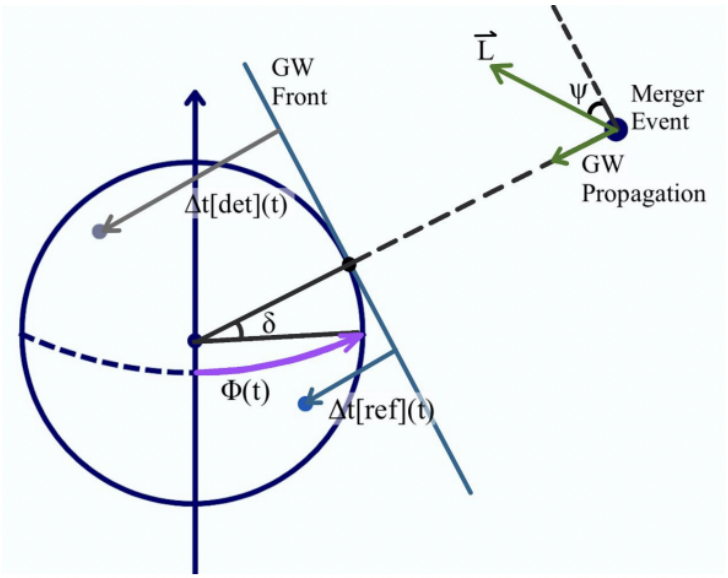

Figure 4: Visual representation of how GW signals are received at Earth. $\Phi(t)$ and δ are sky-location angles, the polarization angle ψ is the angle of projection of the merger's angular momentum $\vec{L}$ onto the GW signal's transverse plane, Δt[det] is the time delay of the signal from some reference Δt[ref].

In a network of detectors, the arrival time of the GW signal at each site varies due to differences in geographic location. Δt, the arrival time of a signal relative to its arrival time at the reference detector (in our case, LIGO Livingston), is critical for localizing the GW source in the sky (see Equation 6).

The angle $\Phi(t)$, representing Earth's rotation, evolves over time as:

$$\Phi(t) = \Phi_0 + \Omega(t - t_0) \tag{3}$$

from some arbitrary starting time t_0, and where Ω is Earth's rotational rate. In a simplified non-rotating Earth model, $\Omega = 0$, so $\Phi(t) = \Phi_0$.

In a rotating Earth model (such as the one in Section 3 of this report), all variables dependent on $\Phi(t)$ inherit time dependence: $F_+(t)$, $F_\times(t)$, $\Delta t(t)$.

2.3 Zeroth Order (in Ω) GW signal model

The strain $h(t)$ measured by a single detector is a linear combination of the two GW polarization components $h_+(t)$ and $h_\times(t)$, scaled by the detector's response coefficients:

$$h(t) = F_+[\text{det}] \cdot h_+(t - \Delta t[\text{det}]) + F_\times[\text{det}] \cdot h_\times(t - \Delta t[\text{det}]) \tag{4}$$

The [det] indicates dependence on a particular detector, which will remain implicit for F_+, $F_\times$, and Δt in most future equations.

Notably, h_+ and $h_\times$ are determined by some set of compact binary merger parameters, θ (these parameters are listed in Section 4).

F_+ and $F_\times$ are given by:

$$F_+ = \vec{X}^T D[\text{det}]\vec{X} - \vec{Y}^T D[\text{det}]\vec{Y}, \quad F_\times = \vec{X}^T D[\text{det}]\vec{Y} + \vec{Y}^T D[\text{det}]\vec{X}, \tag{5}$$

where D is a 3×3 symmetric, constant matrix describing a detector's orientation and location:

$$D \equiv \begin{pmatrix} D_{11} & D_{12} & D_{13} \\ D_{12} & D_{22} & D_{23} \\ D_{13} & D_{23} & D_{33} \end{pmatrix}.$$

The vectors $\vec{X}$ and $\vec{Y}$ are on the transverse plane of a GW:

$$\vec{X} = \begin{pmatrix} \sin\Phi\cos\psi - \sin\psi\cos\Phi\cos\left(\frac{\pi}{2} - \delta\right), \\ -\cos\Phi\cos\psi - \sin\psi\sin\Phi\cos\left(\frac{\pi}{2} - \delta\right), \\ \sin\psi\sin\left(\frac{\pi}{2} - \delta\right) \end{pmatrix},$$

$$\vec{Y} = \begin{pmatrix} -\sin\Phi\sin\psi - \cos\Phi\cos\psi\cos\left(\frac{\pi}{2} - \delta\right), \\ \cos\Phi\sin\psi - \sin\Phi\cos\psi\cos\left(\frac{\pi}{2} - \delta\right), \\ \cos\psi\sin\left(\frac{\pi}{2} - \delta\right) \end{pmatrix}.$$

The time delay Δt of a given detector from the reference detector is given by:

$$\Delta t[\text{det}] = \frac{1}{c}(\vec{r}[\text{det}] - \vec{r}[\text{ref}]) \cdot \vec{e}_{\text{src}}, \tag{6}$$

where:

- $\vec{r} = (x, y, z)$ is the location of a detector relative to the center of the Earth
- The [ref] represents dependence on the reference detector (as opposed to some arbitrary detector indicated by [det]).
- $\vec{e}_{\text{src}}$ is a unit vector aligned in the direction of propagation of the GW, expressed as:

$$\vec{e}_{\text{src}} = \begin{bmatrix} \cos\left(\frac{\pi}{2} - \delta\right)\cos\Phi \\ \cos\left(\frac{\pi}{2} - \delta\right)\sin\Phi \\ \sin\left(\frac{\pi}{2} - \delta\right) \end{bmatrix}$$

- c is the speed of light

To estimate merger parameters θ from LIGO data, we assume that noise in the signal strain is Gaussian-distributed in the frequency domain. Thus, we use GW signal models written in the frequency domain (see Section 4). We can obtain this by taking a Fourier Transform of Equation 4, noting that time-shifts in the time domain result in phase-shifts in the frequency domain (Transform T3):

$$\tilde{h}(f) = \left[F_+\tilde{h}_+(f) + F_\times\tilde{h}_\times(f)\right] e^{-2\pi i f \Delta t} \tag{7}$$

2.4 Why Account for Earth's Rotation?

For current detectors (LIGOs/Virgo), signals typically last $\mathcal{O}(10)$ seconds. During these timescales, Earth's rotation causes only minor variations in detector orientation (F_+, $F_\times$ coefficients) and time delays (Δt between detectors).

However, next-generation detectors will fundamentally change this picture. The GW frequency evolution follows:

$$2\dot{f}_{\mathrm{GW}} = \frac{96}{5}\pi^{8/3}\left(\frac{GM}{c^3}\right)^{5/3}(2f_{\mathrm{GW}})^{11/3} \tag{8}$$

with M being the chirp mass of the binary merger and G the gravitational constant.

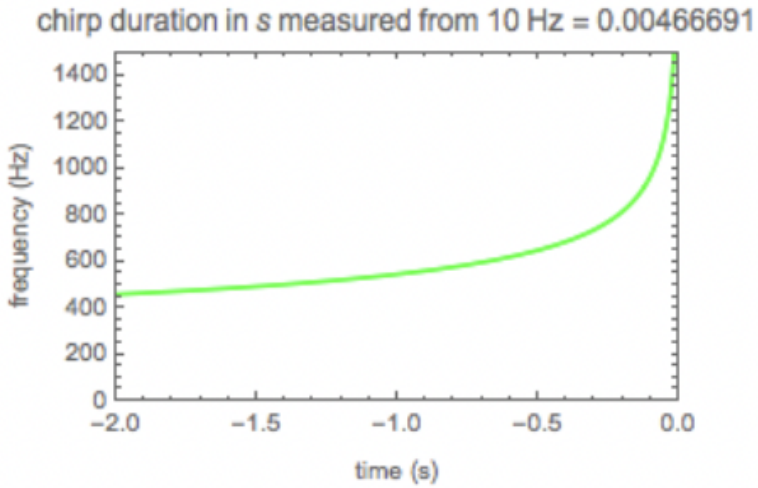

Figure 5: Frequency evolution showing characteristic "chirp" (greater-than-exponential growth) in final moments before merger. Effectively, a plot of $f_{\mathrm{GW}}(t)$ from Equation 8. [4]

As a result, a seemingly small decrease in the cutoff frequency of a detector (that is, the GW signal can be recovered at lower frequencies) will result in a greater than exponential increase in the detectable signal duration!

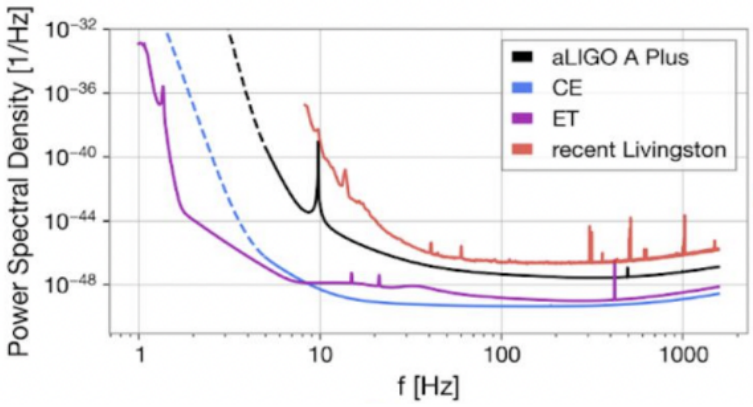

Figure 6: Noise spectra showing improved low-frequency sensitivity [2].

Key differences emerge when comparing detectors:

Parameter	Current	Next-gen
Cutoff frequency	8 Hz	3 Hz
Observable duration	Seconds	Hours

Table 1: Detector capabilities comparison

Thus, with next-gen detectors allowing signal observations on the timescale of hours, Earth's rotation becomes significant.

3 First-Order Perturbative Expansion

3.1 Time Domain Representation

From Equation 3, it is clear that a rotating Earth model must introduce time-dependence to quantities dependent on $\Phi(t)$, including F_+, $F_\times$, and Δt as:

$$h_{\text{rot}}(t) = F_+(t) \cdot h_+(t - \Delta t(t)) + F_\times(t) \cdot h_\times(t - \Delta t(t)) \tag{9}$$

3.1.1 Expansion of key terms in Ω

To account for Earth's rotation, we expand each time-dependent term to first order in Ω, the Earth's rotational rate. This yields linear perturbations around the non-rotating Earth model ($\Omega = 0$):

$$\begin{aligned} F_+(t) &= F_+(t_0) + \Omega \cdot (t - t_0) \cdot \gamma_+, \\ F_\times(t) &= F_\times(t_0) + \Omega \cdot (t - t_0) \cdot \gamma_\times, \\ \Delta t(t) &= \Delta t(t_0) + \Omega \cdot (t - t_0) \cdot \eta, \end{aligned} \tag{10}$$

where γ_+, $\gamma_\times$, and η are constants derived by first order expansions of Equation 5 and Equation 6. Higher order terms in Ω are neglected in this approximation.

To get an idea for what the mathematics behind these expansions look like, let's explore the simplest one: the first order expansion of $\Delta t(t)$. For cleaner notation, we'll use the subscripts d and r to denote positional coordinates of the detector and reference, respectively. Expanding Equation 6 and evaluating it at $t = t_0$:

$$\Delta t(t) = \frac{1}{c}[(x_d - x_r)\cos(\frac{\pi}{2} - \delta)\cos\Phi(t) + (y_d - y_r)\cos(\frac{\pi}{2} - \delta)\sin\Phi(t) + (z_d - z_r)\sin(\frac{\pi}{2} - \delta)]$$

$$\Delta t(t_0) = \frac{1}{c}[(x_d - x_r)\cos(\frac{\pi}{2} - \delta)\cos\Phi_0 + (y_d - y_r)\cos(\frac{\pi}{2} - \delta)\sin\Phi_0 + (z_d - z_r)\sin(\frac{\pi}{2} - \delta)]$$

Per Equation 10, we need to find the difference between the expressions above and factor out $\Omega \cdot (t - t_0)$ to determine η. Evaluating the following two expressions in advance using Equation 3 and a first order expansion in Ω makes this simpler:

$$\cos\Phi(t) - \cos\Phi_0 = \cos(\Phi_0 + \Omega \cdot (t - t_0)) - \cos\Phi_0 \approx -\Omega \cdot (t - t_0) \cdot \sin\Phi_0$$

Similarly,

$$\sin\Phi(t) - \sin\Phi_0 \approx \Omega \cdot (t - t_0) \cdot \cos\Phi_0$$

As planned, we can now calculate η:

$$\Delta t(t) - \Delta t(t_0) = \frac{1}{c}\left[(x_d - x_r)\cos\left(\tfrac{\pi}{2} - \delta\right)(-\Omega \cdot (t - t_0)\sin\Phi_0) + (y_d - y_r)\cos\left(\tfrac{\pi}{2} - \delta\right)(\Omega \cdot (t - t_0)\cos\Phi_0)\right]$$

$$\eta = \frac{1}{c}\cos\left(\tfrac{\pi}{2} - \delta\right)\left[(y_d - y_r)\cos\Phi_0 - (x_d - x_r)\sin\Phi_0\right] \tag{11}$$

The other expansions required are significantly longer, though similar in procedure. While those details will not be covered in this report, the final closed-form expressions for γ_+ and $\gamma_\times$ can be found in Appendix **??**.

3.1.2 Using $F_+(t)$, $F_\times(t)$, $\Delta t(t)$ expansions for first-order perturbation of $h(t)$

Let's focus on expanding $F_+(t) \cdot h_+(t - \Delta t(t))$. The cross-polarization terms will follow similarly.

It is trivial to incorporate the linear perturbations in $F_+(t)$:

$$h_{\text{rot}}(t) = F_+(t_0) \cdot h_+(t - \Delta t(t)) + \Omega \cdot (t - t_0) \cdot \gamma_+ \cdot h_+(t - \Delta t(t)) + (\text{cross terms}) \tag{12}$$

Next, we can expand $h_+(t - \Delta t(t))$ as:

$$h_+(t - \Delta t(t_0) - \eta\Omega \cdot (t - t_0)) \approx h_+(t - \Delta t(t_0)) - \Omega(t - t_0) \cdot \eta \cdot h'_+(t - \Delta t(t_0))$$

Substituting this result into Equation 12, omitting greater-than-linear order terms in Ω, and subtracting the zeroth order model $h_{\text{nonrot}}(t)$ (see Equation 4) yields the following result:

$$\begin{aligned} h_{\text{rot}}(t) - h_{\text{nonrot}}(t) = \Omega(t - t_0)\big[\gamma_+ \cdot h_+(t - \Delta t(t_0)) - \eta \cdot F_+(t_0) h'_+(t - \Delta t(t_0))\big] \\ + (\text{cross terms}). \end{aligned} \tag{13}$$

3.2 Frequency Domain Representation

As explained in Section 2.3, we use GW models in the frequency domain. This necessitates transforming the perturbed strain in Equation 13 to the frequency domain, for which we'll use the following key Fourier identities:

$$t \cdot x(t) \xrightarrow{\mathcal{F}} \frac{i}{2\pi}\frac{\partial}{\partial f}\tilde{x}(f) \tag{T1}$$

$$x'(t) \xrightarrow{\mathcal{F}} 2\pi i f \cdot \tilde{x}(f) \tag{T2}$$

$$x(t - \tau) \xrightarrow{\mathcal{F}} \tilde{x}(f) \cdot e^{-2\pi i f \tau} \tag{T3}$$

Again, we'll focus on the plus terms in our calculation and infer the cross terms. Let's tackle this problem in bits. Using Transform T3:

$$h_+(t - \Delta t(t_0)) \xrightarrow{\mathcal{F}} \tilde{h}_+(f) \cdot e^{-2\pi i f \cdot \Delta t(t_0)}$$

Similarly, using Transform T2:

$$h'_+(t - \Delta t(t_0)) \xrightarrow{\mathcal{F}} 2\pi i f \cdot \tilde{h}_+(f) \cdot e^{-2\pi i f \cdot \Delta t(t_0)}$$

Using the above two transforms, we can deduce from Transform T1:

$$t \cdot h_+(t - \Delta t(t_0)) \xrightarrow{\mathcal{F}} \frac{i}{2\pi}\tilde{h}'_+(f) \cdot e^{-2\pi i f \cdot \Delta t(t_0)} + \Delta t(t_0)\tilde{h}_+(f) \cdot e^{-2\pi i f \cdot \Delta t(t_0)}$$

$$t \cdot h'_+(t - \Delta t(t_0)) \xrightarrow{\mathcal{F}} -\tilde{h}_+(f) \cdot e^{-2\pi i f \cdot \Delta t(t_0)} - f \cdot \tilde{h}'_+(f) \cdot e^{-2\pi i f \cdot \Delta t(t_0)} + 2\pi i f \cdot \Delta t(t_0)\tilde{h}_+(f) \cdot e^{-2\pi i f \cdot \Delta t(t_0)}$$

Having the Fourier transforms of $h_+(t - \Delta t(t_0))$, $t \cdot h_+(t - \Delta t(t_0))$, $h'_+(t - \Delta t(t_0))$, and $t \cdot h'_+(t - \Delta t(t_0))$, it is trivial to compute the Fourier transform of Equation 13. By defining the following constants to simplify notation:

$$\alpha_0 = e^{-2\pi i f \cdot \Delta t(t_0)},$$

$$\alpha_1^+ = \alpha_0\big\{\eta \cdot \Omega \cdot F_+(t_0)\big[1 + 2\pi i f \cdot (t_0 - \Delta t(t_0))\big] - \gamma_+ \cdot \Omega\big[t_0 - \Delta t(t_0)\big] + F_+(t_0)\big\},$$

$$\alpha_2^+ = \alpha_0 \cdot \Omega\left\{\frac{i}{2\pi} \cdot \gamma_+ + \eta \cdot F_+(t_0) \cdot f\right\}.$$

we arrive at a compact frequency-domain representation of the perturbed strain:

$$\tilde{h}_{\text{rot}}(f) = \alpha_1^+ \cdot \tilde{h}_+(f) + \alpha_2^+ \cdot \tilde{h}'_+(f) + \alpha_1^\times \cdot \tilde{h}_\times(f) + \alpha_2^\times \cdot \tilde{h}'_\times(f). \tag{14}$$

Here, $\alpha_1^\times$ and $\alpha_2^\times$ are analogous to their plus-polarization counterparts. The derivatives h'_+ and $h'_\times$ can be computed exactly using automatic differentiation or approximately by finite differencing.

4 Parameter Estimation

There remains one thing to (briefly) explore: how is a gravitational wave model used to conduct parameter estimation? We are given observation $d(f) = h(f, \theta) + n(f)$, where $h(f, \theta)$ is our GW model and $n(f) \sim N(0, \frac{T}{4}S_n(f))$ under the assumption that noise in our data is Gaussian in the frequency domain. $S_n(f)$ represents the spectral noise density (see Figure 6). We use the following Bayesian parameter estimation framework:

$$P(\theta|d) \propto P(d|\theta) \cdot P(\theta) = L(\theta) \cdot P(\theta)$$

where:

- θ represents the merger parameters (chirp mass, spins, location, orientation, tidal deformability for neutron star mergers)
- $P(\theta)$ is the prior probability distribution
- $L(\theta) \equiv P(d|\theta)$ is the likelihood of observing data d given parameters θ

For GW analysis, we compute the log likelihood as a means to obtaining the posterior probability for a certain set of parameters, $P(\theta|d)$, given by:

$$\log L(\theta) = \langle d(f)|h(f, \theta)\rangle - \frac{1}{2}\langle h(f, \theta)|h(f, \theta)\rangle \tag{15}$$

where the inner product is defined as:

$$\langle a|b\rangle = \text{Re}\left\{\sum_f \frac{a^*(f)b(f)}{\frac{T}{2} \cdot S_n(f)}\right\}.$$

T is the observation duration.

The full posterior distribution in θ-space is typically explored computationally via Markov Chain Monte Carlo (MCMC) methods.[5] This allows us to quantify both the most probable parameter values and their uncertainties.

5 Conclusion

With readable signal durations on the order of hours, next-generation detectors will require more than a first-order approximation in Ω to obtain closed-form GW signal estimates. That said, the first-order approximation, Equation 14, will hold where the zeroth order model begins to collapse, making it useful in determining the signal duration at which the zeroth order model's parameter estimations meaningfully diverge from the ground truth. This threshold could equivalently be evaluated in terms of detector frequency cutoff or binary merger chirp mass (see Equation 8). More generally, Equation 14 serves as a good benchmark for how GW strain models perform when the Earth's rotation comes into play.

Future directions for this work include determining second- and higher-order perturbative models, developing a closed form solution for $\tilde{h}_{rot}(f)$, and deep-learning based techniques for parameter estimation. More advanced models may also incorporate other dynamic effects such as tidal distortions or non-uniform rotational influences. Ultimately, bridging the gap between theory and practical detection demands a continued refinement of our models—ensuring that next-generation detectors can fully realize their potential in detecting compact binary mergers.

References

[1] Imène Belahcene. *Searching for gravitational waves produced by cosmic strings in LIGO-Virgo data*. PhD thesis, 10 2019.

[2] M. Lazarow, N. Leslie, and L. Dai. A gravitational waveform model for detecting accelerating inspiraling binaries. *arXiv*, 2024. arXiv:2401.04175.

[3] LIGO Laboratory. Ligo's interferometers. https://www.ligo.caltech.edu/page/ligos-ifo, n.d. Accessed: 2025-05-08.

[4] Satya Mohapatra. Newtonian gravitational wave chirp signal from merger of a compact binary. https://demonstrations.wolfram.com/NewtonianGravitationalWaveChirpSignalFromMergerOfACompactBin/, 2011. Wolfram Demonstrations Project.

[5] Joshua S. Speagle. A conceptual introduction to markov chain monte carlo methods, 2020.